

An Interactive Pipeline for Quantitative Histopathological Analysis of Spatially Defined Drug Effects in Tumors

Sebastian W Ahn¹, Benjamin Ferland¹, Oliver H Jonas¹

¹Department of Radiology, Laboratory for Bio-Micro Devices, Brigham and Women's Hospital, Boston, MA, USA

Submitted: 03-Mar-2021

Revised: 10-May-2021

Accepted: 10-May-2021

Published: ***

Abstract

Background: Tumor heterogeneity is increasingly being recognized as a major source of variability in the histopathological assessment of drug responses. Quantitative analysis of immunohistochemistry (IHC) and immunofluorescence (IF) images using biomarkers that capture spatial patterns of distinct tumor biology and drug concentration in tumors is of high interest to the field. **Methods:** We have developed an image analysis pipeline to measure drug response using IF and IHC images along spatial gradients of local drug release from a tumor-implantable drug delivery microdevice. The pipeline utilizes a series of user-interactive python scripts and CellProfiler pipelines with custom modules to perform image and spatial analysis of regions of interest within whole-slide images. **Results:** Worked examples demonstrate that intratumor measurements such as apoptosis, cell proliferation, and immune cell population density can be quantitated in a spatially and drug concentration-dependent manner, establishing *in vivo* profiles of pharmacodynamics and pharmacokinetics in tumors. **Conclusions:** Spatial image analysis of tumor response along gradients of local drug release is achievable in high throughput. The major advantage of this approach is the use of spatially aware annotation tools to correlate drug gradients with drug effects in tumors *in vivo*.

Keywords: Controlled release, digital pathology, image annotation, quantitative pathology, spatial analysis, tumor microenvironment

INTRODUCTION

The spatial aspect of cancer biology and drug response is becoming increasingly prominent as we recognize that the function of cells, and the activity of drugs, is determined not only by the state and prevalence of certain cell types but also by their location and environment within complex tissues.

In oncology, heterogeneous drug responses are common, with pockets of tumor showing significant cell kill from chemotherapeutic agents, while other areas of the tumor appear to be resistant.^[1,2] This is in due in part to inherent molecular aberrations that are present in only a subset of cells, as well as specific resistance factors in the tumor microenvironment such as distinct cell types (e.g., M2 macrophages), growth factors,^[3,4] or bacteria.^[5] Another significant driver of heterogeneous drug responses is the unequal distribution of the drug itself within the tumor during clinical dosing. This creates gradients of drug concentration that correlates with physiological features of the tumor such as vasculature.^[6,7] The observed patterns of spatial heterogeneity of drug responses within the same tumor

create a need to analyze local drug responses within the tumor in a manner that takes into account such spatial features and gradients.

Drug-eluting implants represent a major advancement to diagnose and treat a variety of cancers^[8] and other diseases.^[9,10] Such implants release drugs into specific regions of tumors or other tissues and thus create a regionalized effect. In cardiovascular applications, drug-eluting stents also exhibit similar spatial patterns of drug release.^[11,12] The concentration profiles of drugs in this setting are typically distance-dependent gradients from the site of release. Whether gradients of drug release and tissue response are caused by heterogeneity in tumor physiology during standard clinical systemic dosing, or

Address for correspondence: Dr. Oliver Jonas,

Department of Radiology, Laboratory for Bio-Micro Devices, Brigham and Women's Hospital, 221 Longwood Avenue, RM 429, Boston, MA 02115, USA.

E-mail: ojonas@bwh.harvard.edu

Access this article online

Quick Response Code:



Website:
www.jpathinformatics.org

DOI:
10.4103/jpi.jpi_17_21

This is an open access journal, and articles are distributed under the terms of the Creative Commons Attribution-NonCommercial-ShareAlike 4.0 License, which allows others to remix, tweak, and build upon the work non-commercially, as long as appropriate credit is given and the new creations are licensed under the identical terms.

For reprints contact: WKHLRPMedknow_reprints@wolterskluwer.com

How to cite this article: Ahn S, Ferland B, Jonas O. An interactive pipeline for quantitative histopathological analysis of spatially defined drug effects in tumors. *J Pathol Inform* 2021;XX:XX-XX.

by implantable drug delivery systems, traditional histological analyses that average effects over entire tissue sections miss critical features of drug response that may have clinical impact. To accurately determine the efficacy of a drug which is inherently dose-dependent, one must take into account the spatial orientation and concentration differences of the drug in the target organ.

There have been key advancements in the development of novel experimental techniques using spatially conserved approaches to measure drug responses of tumors and other tissues. These approaches are able to analyze specific regions of tissues based on their defined location in the organ. Examples include spatial transcriptomics and proteomics, with multiple platforms becoming available.^[13,14] The gold standard for clinical diagnoses remains histopathological analysis by H&E and immunohistochemistry (IHC)/immunofluorescence (IF), but quantitative approaches that take into account spatial drug gradients and physiological features are currently lacking.

There is a significant need to analyze and quantitative histopathological data in an analogous spatially confined and preserved manner. To this end, we have developed an annotation pipeline utilizing python, CellProfiler, and other methods that are capable of allowing users to define specific regions within a whole tumor section and creating regions of interest (ROIs) that correspond to drug delivery regions eluted from an implantable microdevice used for intratumor delivery of chemotherapeutic agents. The pipeline is capable of quantitating cellular markers from IHC- or IF-stained slides for a large variety of markers and provides direct quantitative measurement of drug effect in a distance and drug concentration-dependent manner.

METHODS

Histological processing and slide preparation

Samples implanted with microdevices are prepared and processed using established histology workflows as shown in Figure 1.^[15] Slides are then stained and scanned on standard equipment such as Leica Bond autostainers, with images stored locally on a workstation for image processing.

To determine drug release directions at a specific level of an embedded microdevice, a fiducial is used as a reference point for each microdevice. Fiducials can be a feature of the microdevice (e.g., a notch that is identifiable during paraffin block sectioning), or a fluorescent marker compound or drug released unilaterally, which can be detected on an unstained serial section. It can also be a physiological feature of the tumor such as a blood vessel, or a tumor region defined by histological markers such as for proliferation, hypoxia, or stromal content. Once the angle of the fiducial is determined for an embedded microdevice, the angles of all other drugs can be derived.^[15]

To investigate the impact of local drug diffusion within whole-slide images (WSI), we outline below the procedure

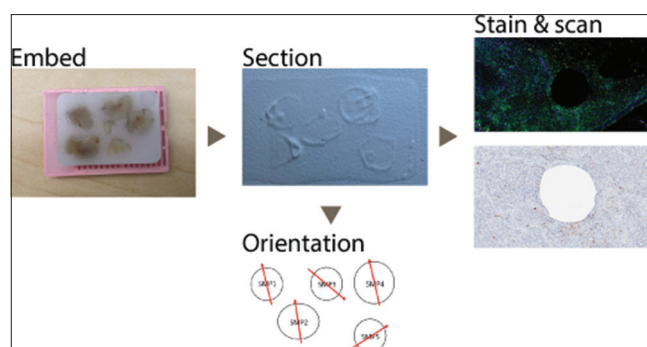


Figure 1: Histology workflow. Several samples implanted with devices are embedded, sectioned, stained, and scanned, with an annotation step for determining device orientation..

for (1) managing blocks, slides, samples, and devices, (2) defining and extracting ROIs, (3) applying cell segmentation and measuring biomarker intensities for individual objects, and then, (4) imposing a spatial context upon the cells within the ROIs.

Project structure

As a project may contain hundreds of slides, project data is stored in a structured hierarchy, as shown in Figure 2a. A given project is comprised of multiple blocks, each containing serial sections for each level of the implanted microdevices. This hierarchy assists in maintaining the relationships between serial sections from the same paraffin block, as microdevice positions and angles are conserved from section to section. Projects may be structured differently, provided the image analysis pipeline is adjusted accordingly.

All WSIs are stored in a folder named “slides;” snapshots of red-green-blue (RGB) images are acquired (e.g., using Aperio ImageScope) and are stored in a folder named “snapshots;” snapshots that are optionally merged and renamed with a unique identifier (e.g., drug) are stored in the “regions” folder; regions that have been annotated by CellProfiler are stored in the “regions_{annotation name}” folder. Specific names in quotation marks are arbitrary and can be adjusted by the user.

Metadata associated with a project include two regular expressions (regexes) and device layouts. Device layouts specify drug locations near a device in cylindrical coordinates, as determined by their level and angle. These metadata are contained in a “project.json” file, as shown in Figure 2b.

The two regexes aid reading and manipulating images when developing scripts and are used for matching and extracting metadata from snapshot and region filenames. To guarantee uniqueness within a project, snapshot filenames must contain the following fields in some order: “project,” “block,” “level,” “panel,” “sample” (e.g., ‘PROJ1_BLK1_LVL1_PANEL1_SMP1.tif’); region filenames must additionally contain “drug” (e.g., “PROJ1_BLK1_LVL1_PANEL1_SMP1_DRUG1.tif”). The regexes corresponding to the above filenames in Python’s regex syntax are “^(?P<project> [A-Za-z0-9-]+)_(?P<block> [A-Za-z0-9-+]+)_LVL(?P<level> [0-9]

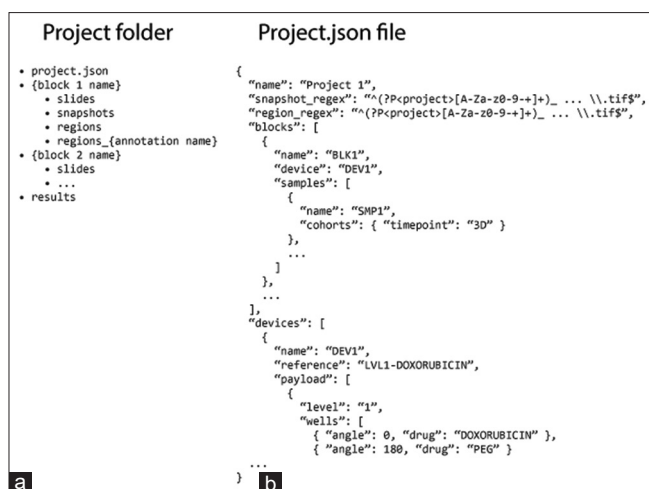


Figure 2: Project folder layout (a) and project.json file structure (b) for a sample project

`+(?P < panel> [A-Za-z0-9] +)_(?P < sample> [A-Za-z0-9] +)\\.tif$` and `^(?P < project> [A-Za-z0-9-] +)_(?P < block> [A-Za-z0-9-+] +)_LVL(?P < level> [0-9] +)_(?P < panel> [A-Za-z0-9] +)_(?P < sample> [A-Za-z0-9] +)_(?P < drug> [A-Za-z0-9-+%]+)\\.tif$`, respectively, and the exact allowable characters in each matching group may be adjusted accordingly.

Cropping regions of interest

As up to as many as ten microdevice-implanted samples may be embedded in a single paraffin block, the resulting WSIs contain numerous, irregularly shaped ROIs. To obtain these regions, we use Aperio ImageScope, a program for visualizing and annotating WSIs from Leica slide-scanning microscopes.

Several aspects of the cropping step are established before any cropping is done. A magnification level that allows ROIs to fit on a single monitor is chosen; typically, $\times 5$ magnification is sufficient to capture the implant hole and surrounding regions of drug diffusion. Brightness and contrast are set to default values (zero) for consistency within slide batches. The filename assigned to the snapshots must follow the user-defined regular expression as defined in the project.json file.

For each sample within a slide, a ROI is defined by a specific morphological feature (e.g., location of device implant, biomarker expression, or other tumor morphological feature). In our case, the center of the device implant serves as a location marker for drug release. Using this point as origin, we specify the magnification level, take a screenshot, and save the screenshot according to the filename format described above.

WSIs with more than three channels, as is the case with most multiplexed immunofluorescence images, require a modification to the above procedure. The snapshot feature in ImageScope generates RGB images directly from the program viewport. If four or more colors are used, additional snapshots (one per each additional set of three channels) are taken per sample. This is a particular limitation of ImageScope

which may not arise if other software tools are used for ROI extraction.

Image preprocessing

Images are preprocessed using a set of python scripts, as shown in Figure 3a.

Step one of the python scripts merges the RGB snapshots stored in the “snapshots” folder into a single multichannel image, identifies the number of regions of drug diffusion within the image using the project.json file, creates the appropriate number of copies of files, appends the drug name to the filename, and saves them to the “regions” folder. The number of copies created depends on the number of drugs released at a particular level of the microdevice.

Step two of the python script reads in a comma-separated values (CSV) file (or creates one if it does not exist), modifies it, and saves it. The CSV file consists of filenames and two pairs of points for each filename, one for the center of the reservoir and the other for the center of curvature. For each filename, the script renders the image, a user-interactive bow using the two pairs of points, and buttons for marking whether to include or exclude the image, for quality control purposes [Figure 4]. The two pairs of points are marked by crosses and can be adjusted by the user to annotate the position and direction of drug diffusion. The bow direction is determined by summing the angle of the microdevice’s fiducial and the relative angle between the fiducial and the drug.

Step three of the python script makes minor modifications to the CSV file for input into CellProfiler.

Image processing

ROIs extracted from WSIs, along with metadata in the associated CSV file, are input into CellProfiler^[16] for image and spatial processing. The construction of the CellProfiler pipeline depends on the imaging modality used [Figure 3b]. For brightfield images, a spectral deconvolution step resolves the image into the individual dyes (e.g., hematoxylin, DAB). For multichannel images, the image stack can be split using *ColorToGray* directly into the corresponding biomarkers. Nuclear objects are computed by running the *IdentifyPrimaryObjects* module on the nuclear image and cellular objects from nuclear objects using the *IdentifySecondaryObjects* module. The *MakeWedgeMask* CellProfiler module generates a binary mask from the well and center points to filter segmented objects of interest. The *MakePaddedMask* CellProfiler module generates a rectangular mask expanded out from the wedge mask to aid in cropping and minimizing extraneous image processing.

Spatial processing

Associated with each region of drug diffusion are two points that determine the reservoir, one for the center of the reservoir and one for the center of curvature. Imposing a polar coordinate system based on these two points enables distance-dependent profiling of the segmented objects [Figure 5]. A custom CellProfiler module (*MeasureObjectDistanceFromReservoir*)

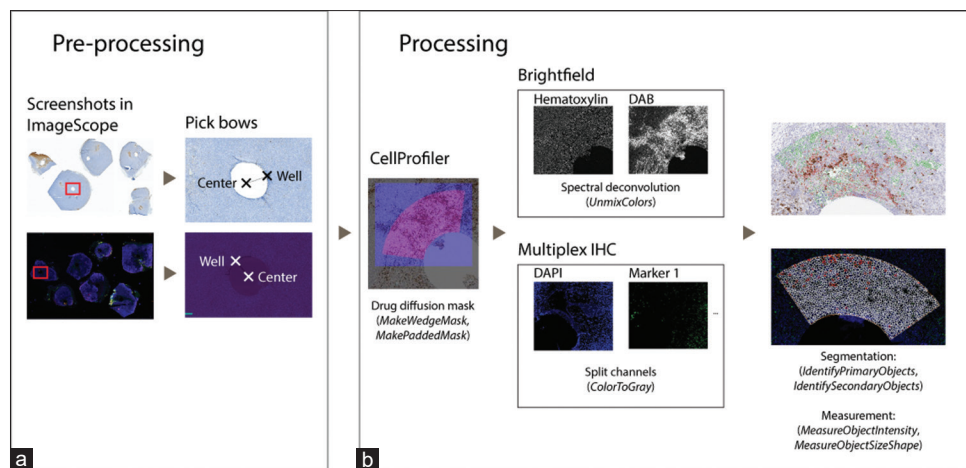


Figure 3: Image (pre) processing. Cropped images are annotated with the well position and angle using the device orientations (a), and analyzed using the appropriate CellProfiler pipeline (b). Names of CellProfiler modules are indicated in italics.

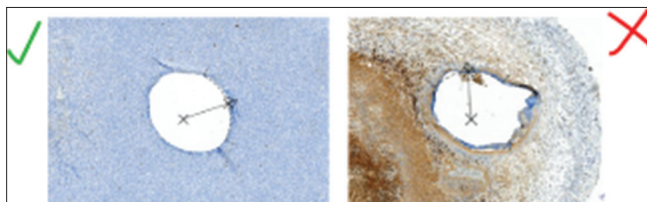


Figure 4: Quality control. Images of areas with poor tissue integrity or drug release outside of the desired tissue are excluded.

was written to measure the azimuthal and radial position of objects relative to the bow coordinates.

Direct/indirect measurements of drug concentration can be obtained using other imaging modalities and registered with IHC/IF images to obtain the correlation between drug concentration and drug effect. If unavailable, the distance of a cell or pixel to the drug reservoir edge can serve as a proxy for drug concentration.

Worked examples

Project preparation

This study was performed in strict accordance with IACUC-approved protocol 2017N000003 at Brigham and Women's Hospital.

Tumors injected with ovarian cancer cells to form patient-derived xenografts were loaded with the payload as shown in Figure 6 for 24 h. Samples were obtained from sacrificed mice and formalin-fixed and paraffin-embedded (FFPE). Five- μ m sections were obtained from paraffin blocks, stained with cleaved caspase 3 (rabbit monoclonal, clone 5A1E, catalog no. 9664, dilution 1/300; Cell Signaling) against diaminobenzidine (DAB), and counterstained with hematoxylin.

Tumors grown from the MC38 breast cancer metastasis cell line in mice were implanted with microdevices loaded with the payload as shown in Figure 6 for 7 days. Samples were explanted from sacrificed mice and FFPE. Five- μ m

sections were obtained from paraffin blocks and stained with an antibody panel consisting of the following biomarkers: DAPI (NucBlue R37606, Invitrogen); F4/80 (rabbit monoclonal, clone D2S9R, catalog no. 70076, dilution 1/250; Cell Signaling); STAT1 (rabbit monoclonal, clone D1K9Y, catalog no. 14994, dilution 1/3000; Cell Signaling); Arginase-1 (rabbit monoclonal, clone D4E3M, catalog no. 93668, dilution 1/100; Cell Signaling); and PD-L1 (rabbit monoclonal, clone D5V3B, catalog no. 64988, dilution 1/100; Cell Signaling), and counterstained with DAPI. All IHC was performed on the Leica Bond RX automated staining platform.

Regions of doxorubicin diffusion in serial sections were imaged using the Revolve microscope (Echo Labs) in fluorescence mode.

The project.json files for the two sets of slides above are constructed as shown in Figures 6c and 7c. The complete contents of both files are available in the supplementary section.

Image processing

Figure 8 demonstrates two main use cases of the image analysis pipeline. Tumor sections from Level 5 of the ovarian PDX dataset and Level 9 of the MC38 dataset were picked for these examples.

Fiducial directions for the implanted microdevices in each block were annotated using arrows (8-1). ROIs within slides were identified and cropped using ImageScope's snapshot tool (8-2), then merged with a python script if necessary (8-2a). The drug reservoir edge location and direction were annotated using Step 3 of the python script (8-3). IHC/IF images were registered with fluorescent images of doxorubicin diffusion from serial sections using the interactive similarity plugin in ImageJ.

Annotated images were input into CellProfiler, and the appropriate pipelines for each imaging modality were constructed. To begin, the *MakeWedgeMask* and

MakePaddedMask modules generated binary masks for filtering objects of interest and for minimizing the processed portion of images (8-4a).

For the CC3 panel [Figure 8a], images were unmixed using the *UnmixColors* module into the DAB and hematoxylin channels. To quantify apoptosis, a threshold approach was used instead of object segmentation, as the signal appeared highly acellular and irregular, posing difficulties for nucleus/cell segmentation. The apoptotic index was measured as the ratio of the area of CC3-positive pixels divided by the area of tissue-positive pixels.

For the macrophage panel [Figure 8b], images were split using the *SplitChannels* module into six grayscale images. The *IdentifyPrimaryObjects* and *IdentifySecondaryObjects* modules were used to segment nuclei and cells, and the *MeasureObjectSizeShape* module was used to measure the mean intensities of the six channels for each object, and the *MeasureObjectDistanceFromReservoir* module was used to measure each object's angular and radial distance from the reservoir.

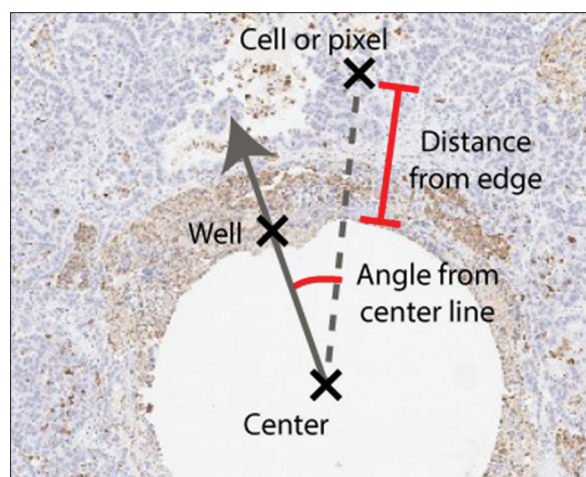


Figure 5: Spatial processing. Segmented objects and areas are profiled as a function of distance.

All data were exported to CSV files using the *ExportToSpreadsheet* module.

Spatial processing

All histograms in Figures 5–8 were weighted using the inverse of the pixel or object distance to center, to account for the linear dependence of pixel or object count on distance to center. For the brightfield panel, pixels were binned by distance, with the following metrics computed per bin: ratio of CC3-positive pixels to total pixels; total intensity of doxorubicin. For the multiplex immunofluorescence panel, cells were binned by distance, with the following metrics computed per bin: number of cells; total pixel intensity of doxorubicin; F4/80⁺ cells out of all cells; STAT-1⁺ cells out of F4/80⁺ cells; Arginase-1⁺ cells out of F4/80⁺ cells; PD-L1⁺ cells out of F4/80⁺ cells.

DISCUSSION

The objective of our work was to create a pipeline for high-throughput analysis of IHC and IF images from spatially defined regions of multiple tumor sections, with a particular focus on integrating drug release gradients with pharmacodynamics (PD) effects. Results demonstrate that spatially-aware measurements are achievable using a semiautomated, user-assisted image analysis pipeline featuring custom python scripts and CellProfiler modules that both guide precise identification of and profile regions based on distance from drug-delivering microdevices. Specifically, we showed that spatial processing of tumor PD markers along drug diffusion gradients offers a quantitative description of *in vivo* changes in cell population densities for a variety of cell types and markers in a drug concentration-dependent manner.

Many existing software tools for annotating WSIs, including ImageJ, Aperio ImageScope, QuPath, and Indica Labs' HALO support common geometries such as points, lines, polygons, and ellipses. However, the geometry of the drug gradients generated about microdevices necessitated the development and use of custom tools. Our method may also guide others in developing their own tools for bespoke applications.

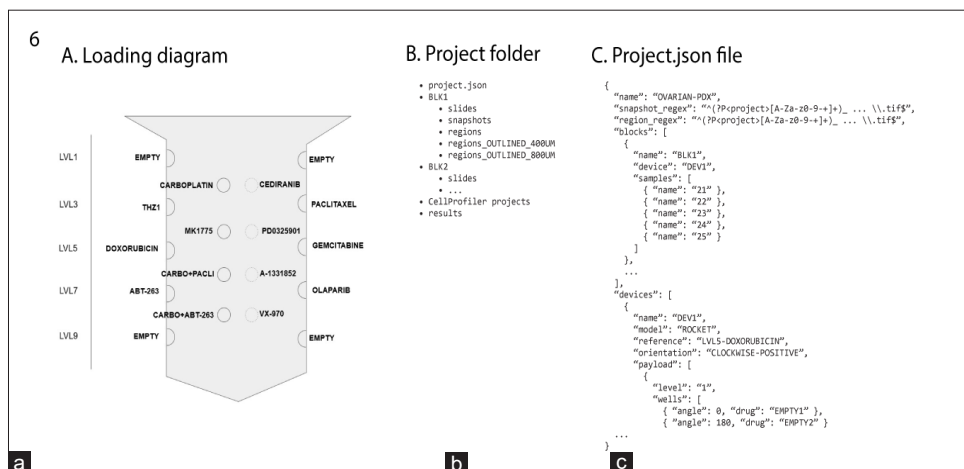


Figure 6: Device loading diagram (a), project folder layout (b), and project.json file structure (c) for the ovarian PDX dataset.

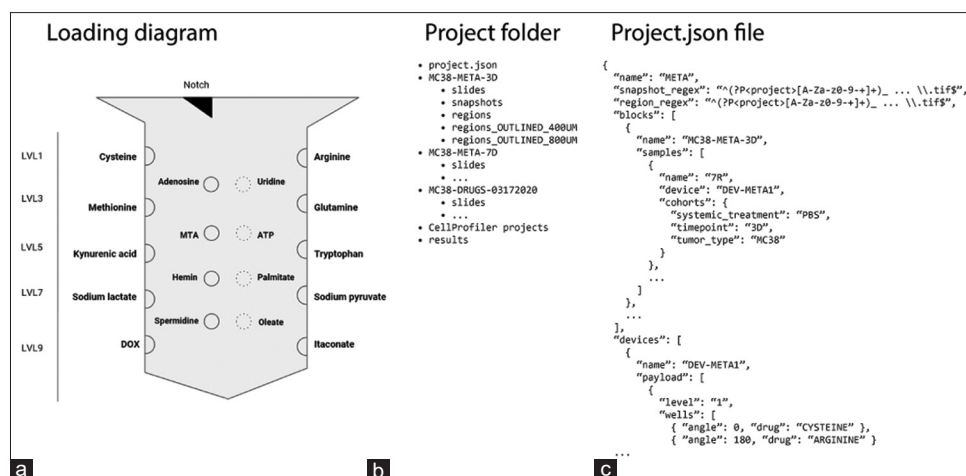


Figure 7: Device loading diagram (a), project folder layout (b), and project.json file structure (c) for the MC38 dataset.

The advantages of multiplex histochemical techniques apply to our method: populations of cell phenotypes defined by colocalization of specific biomarkers can be quantified in terms of distance from the drug release reservoir. For instance, we show that macrophage polarization, which is associated with favorable drug responses in tumors, can be assessed by comparing populations of F4/80⁺/Arginase-1⁺ cells (indicating M2 polarization) with F4/80⁺/Stat-1⁺ cells (indicating M1 polarization).^[17] Various macrophage subpopulations as a function of distance and drug concentration are shown in Figures 5b-8. Analogously, characterization of drug effect-dependent T-cell aggregation in tumors can be assessed using functional lymphocyte markers such as CD3, CD4, CD8, and FoxP3.

A performance metric for the method is estimated time requirement. A typical microdevice project may encompass 36 therapy conditions, each measured in six-fold replicates (216 ROI images) across 18 IF markers, for a total of 3,888 individual drug response phenotypes. For each image, one or more snapshots are acquired by toggling channels and cropping in ImageScope, each of which requires ~30s. For each image, bow orientation for an individual drug phenotype measurement requires ~10–20s, and the decision to include or exclude is usually ~1s but may take up to 5s. The total estimated cropping and annotation time is approximately 9–12 h. The execution time of the CellProfiler pipelines is dependent on the number of available cores and central processing unit speed but remains minor compared to the manual cropping and annotation time. On our workstation (Intel Core i9-7900X at 4.30 GHz, 20 logical processors), image processing for the project described above would finish in under 20 min.

We estimate that a total turnaround time of up to 2 weeks would be allowable for integrating the data output into clinical decision-making on which chemotherapies to prioritize for treatment. This estimate is based on published turnaround times of 2 weeks for genomic assays that predict drug sensitivity, such as FoundationOne PCDx.^[18] Allocating 1 week for sample processing, sectioning, antibody staining, and imaging would

allow one additional week for completing the computational pipeline described here, which is already feasible. Shortening of manual input times would nonetheless be desirable for more routine clinical use, as well as to reduce demand on personnel.

Several key future areas of improvement have been identified. Most notably, we anticipate that image processing and machine learning feature recognition algorithms can be used to identify microdevice and reservoir positions and orientations within a tissue section. Combined with the constraints that microdevice locations and orientations are essentially fixed with respect to each other from serial section to serial section within a paraffin block, and that reservoir orientations are rigidly positioned about the microdevice, deployment of these algorithms would eliminate nearly all manual annotation tasks, only potentially requiring minor adjustments.

Another area of improvement is integration with WSI analysis software. The software may operate directly on the underlying pixel data and directly manage annotations, eliminating time-and memory-intensive cropping operations as well as the directory structure and CSV files described above. At present, ImageScope itself is not used for image analysis, as it is proprietary and difficult to extend; open-source programs such as QuPath and Napari are potential candidates.

Moreover, our method is sensitive to artifacts from the standard histology workflow (e.g., dust, out-of-focus regions, uneven staining, and folds and tears in tissue). Such confounding effects may impinge upon ROIs and bias measurement operations. Instead of excluding entire ROIs, as is currently done, undesired artifacts may be removed using polygon-or pixel-based annotation tools or machine vision methods.^[19,20] Variations in staining may be reduced by maintaining stringent histology standards, including embedding samples close to each other within a given paraffin block, avoiding placing tissue sections close to coverslip edges, consistent sample preparation and fixation, antibody validation, and slide staining and scanning in batches.^[21]

Additional depth in analysis and measurement may be introduced. Spatial analysis algorithms, inspired by the

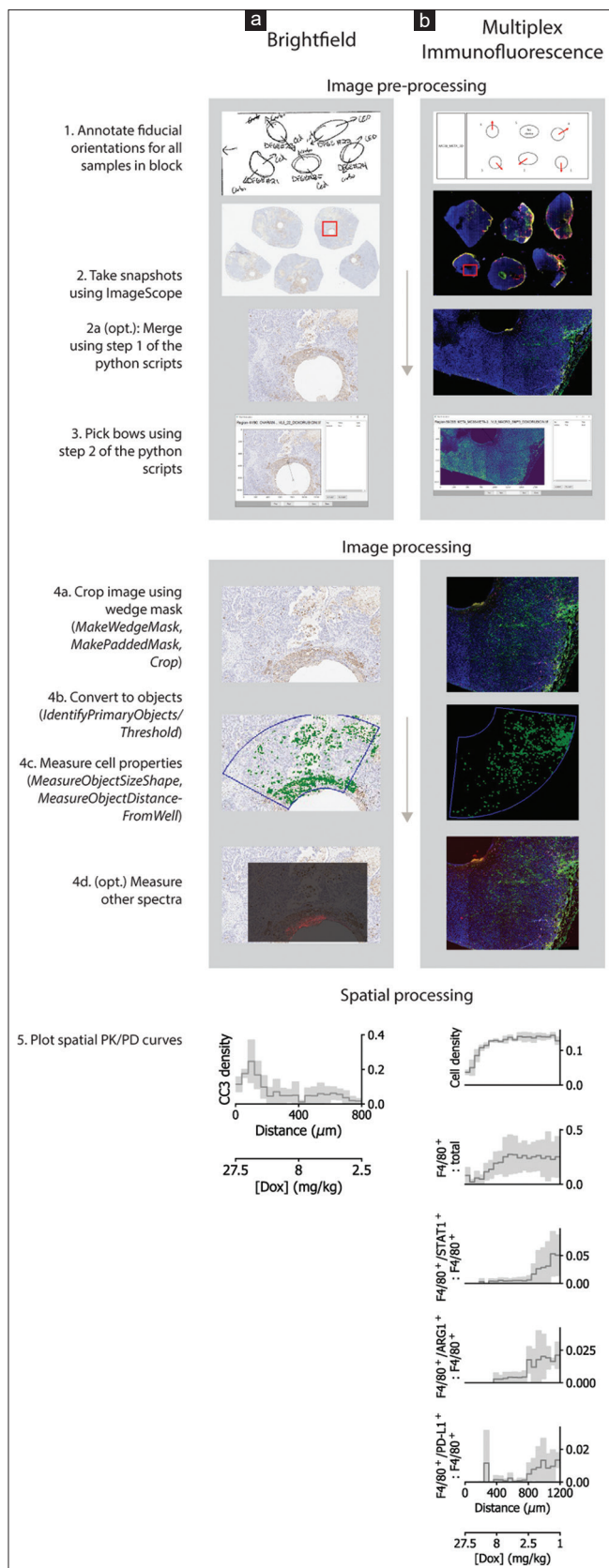


Figure 8: Image and spatial processing for brightfield (8a) and multiplex immunofluorescence (8b) whole-slide images.

geospatial and ecology analysis community, could further enhance drug concentration-dependent cell–cell interaction analysis.^[22–25] Image registration with other modalities such as imaging mass spectroscopy and spatial transcriptomics may offer additional mechanistic insight by integrating biological readouts from different modalities.^[26,27]

We envision that this pipeline will enable *in vivo* pharmacokinetic (PK) and PD profiling of drug action, not only in tumors but also in any solid tissue. Notably, in combination with the availability of up to twenty reservoirs on a drug-delivering microdevice, the pipeline may fuse *in vivo* mechanistic insight from the pharmacologic space with the spatial, temporal, and omics spaces, potentially enabling deep, tailored precision therapy response measurement.

CONCLUSIONS

We present here an integrated image analysis pipeline consisting of custom python scripts and CellProfiler pipelines that guide annotation of regions of drug diffusion. The pipeline allows users to profile the spatial effects of local drug diffusion in microdevice-implanted tumors in high throughput, essentially generating PK/PD quantitation for multiple drugs and tissue regions from a given tumor. The pipeline enables spatial profiling by moving from polygons to custom annotation tools, allowing correlation of drug gradients with drug effects in the context of the tumor microenvironment. The addition of *in vivo* mechanistic insight enables quantitative analysis of tumor response as measured by multiple markers with drug release gradients, tissue heterogeneity, and other spatial aspects of tumor physiology.

Code

The python scripts are available at <https://github.com/biomicrodev/antilles>. The custom CellProfiler modules are available at <https://github.com/biomicrodev/jonaslab-cpp>.

Acknowledgments

Funding for this study was provided by NIH grants R01CA223150, R37CA224144, and R33CA223904. We thank Dana-Farber/Harvard Cancer Center in Boston, MA, for the use of the Specialized Histopathology Core and the Tissue Microarray Imaging Core, which provided histology, immunohistochemistry, and imaging services.

Financial support and sponsorship

Nil.

Conflicts of interest

There are no conflicts of interest.

REFERENCES

1. Trédan O, Galmarini CM, Patel K, Tannock IF. Drug resistance and the solid tumor microenvironment. *J Natl Cancer Inst* 2007;99:1441–54.
2. Galmarini CM, Galmarini FC. Multidrug resistance in cancer therapy: Role of the microenvironment. *Curr Opin Investig Drugs* 2003;4:1416–21.

3. Straussman R, Morikawa T, Shee K, Barzily-Rokni M, Qian ZR, Du J, *et al.* Tumour micro-environment elicits innate resistance to RAF inhibitors through HGF secretion. *Nature* 2012;487:500-4.
4. Wilson TR, Fridlyand J, Yan Y, Penuel E, Burton L, Chan E, *et al.* Widespread potential for growth-factor-driven resistance to anticancer kinase inhibitors. *Nature* 2012;487:505-9.
5. Geller LT, Barzily-Rokni M, Danino T, Jonas OH, Shental N, Nejman D, *et al.* Potential role of intratumor bacteria in mediating tumor resistance to the chemotherapeutic drug gemcitabine. *Science* 2017;357:1156-60.
6. Minchinton AI, Tannock IF. Drug penetration in solid tumours. *Nat Rev Cancer* 2006;6:583-92.
7. Fusco Nerini I, Morosi L, Zucchetti M, Ballerini A, Giavazzi R, D'Incalci M. Intratumor heterogeneity and its impact on drug distribution and sensitivity. *Clin Pharmacol Ther* 2014;96:224-38.
8. Shapira-Furman T, Serra R, Gorelick N, Doglioli M, Tagliaferri V, Cecia A, *et al.* Biodegradable wafers releasing Temozolomide and Carmustine for the treatment of brain cancer. *J Control Release* 2019;295:93-101.
9. Farra R, Sheppard NF Jr., McCabe L, Neer RM, Anderson JM, Santini JT Jr., *et al.* First-in-human testing of a wirelessly controlled drug delivery microchip. *Sci Transl Med* 2012;4:122ra21.
10. Saito Y, Kobayashi Y. Contemporary coronary drug-eluting and coated stents: A mini-review. *Cardiovasc Interv Ther* 2021;36:20-2.
11. Tzafiriri AR, Groothuis A, Price GS, Edelman ER. Stent elution rate determines drug deposition and receptor-mediated effects. *J Control Release* 2012;161:918-26.
12. Balakrishnan B, Dooley JF, Kopia G, Edelman ER. Intravascular drug release kinetics dictate arterial drug deposition, retention, and distribution. *J Control Release* 2007;123:100-8.
13. Turczyk BM, Busby M, Martin AL, Daugherty ER, Myung D, Terry RC, *et al.* Spatial Sequencing: A Perspective. *J Biomol Tech* 2020;31:44-6.
14. Maniatis S, Petrescu J, Phatnani H. Spatially resolved transcriptomics and its applications in cancer. *Curr Opin Genet Dev* 2021;66:70-7.
15. Jonas O, Landry HM, Fuller JE, Santini JT Jr., Baselga J, Tepper RI, *et al.* An implantable microdevice to perform high-throughput *in vivo* drug sensitivity testing in tumors. *Sci Transl Med* 2015;7:284ra57.
16. McQuin C, Goodman A, Chernyshev V, Kamensky L, Cimini BA, Karhohs KW, *et al.* CellProfiler 3.0: Next-generation image processing for biology. *PLoS Biol* 2018;16:e2005970.
17. Sica A, Bronte V. Altered macrophage differentiation and immune dysfunction in tumor development. *J Clin Invest* 2007;117:1155-66.
18. Weiss GJ, Hoff BR, Whitehead RP, Sangal A, Gingrich SA, Penny RJ, *et al.* Evaluation and comparison of two commercially available targeted next-generation sequencing platforms to assist oncology decision making. *Onco Targets Ther* 2015;8:959-67.
19. Agarwal N, Xu X, Gopi M. automatic detection of histological artifacts in mouse brain slice images. *Med Comput Vis Bayesian Graph Model Biomed Imaging* 2017;10081 LNCS:105-115.
20. Kothari S, Phan JH, Wang MD. Eliminating tissue-fold artifacts in histopathological whole-slide images for improved image-based prediction of cancer grade. *J Pathol Inform* 2013;4:22.
21. True LD. Quality control in molecular immunohistochemistry. *Histochem Cell Biol* 2008;130:473-80.
22. Stoltzfus CR, Filipek J, Gern BH, Olin BE, Leal JM, Wu Y, *et al.* CytoMAP: A spatial analysis toolbox reveals features of myeloid cell organization in lymphoid tissues. *Cell Rep* 2020;31:107523.
23. Velázquez E, Martínez I, Getzin S, Moloney KA, Wiegand T. An evaluation of the state of spatial point pattern analysis in ecology. *Ecography* 2016;39:1042-55.
24. Arnol D, Schapiro D, Bodenmiller B, Saez-Rodriguez J, Stegle O. Modeling cell-cell interactions from spatial molecular data with spatial variance component analysis. *Cell Rep* 2019;29:202-11.e6.
25. Lun XK, Zanotelli VR, Wade JD, Schapiro D, Tognetti M, Dobberstein N, *et al.* Influence of node abundance on signaling network state and dynamics analyzed by mass cytometry. *Nat Biotechnol* 2017;35:164-72.
26. Van de Plas R, Yang J, Spraggins J, Caprioli RM. Image fusion of mass spectrometry and microscopy: A multimodality paradigm for molecular tissue mapping. *Nat Methods* 2015;12:366-72.
27. Hériché JK, Alexander S, Ellenberg J. Integrating imaging and omics: Computational methods and challenges. *Annu Rev Biomed Data Sci* 2019;2:175-97.